FE Analysis on Temperature, Electromagnetic Force and Load Capacities of Imperfect Assembled GIB Plug-in Connectors

Xiangyu Guan [1], Xin Wei [1], Xianyong Song [2], Naiqiu Shu [1], and Hui Peng [1]

[1] School of Electrical Engineering
Wuhan University, Wuhan, 430072, China
xiangyuguan1986@163.com

[2] State Grid Hunan Power Supply Company
Yue yang, 414000, China
582583392@qq.com

Abstract ─ For purpose of providing effective method of optimal design and failure prediction of plug-in power connector with imperfect assembly conditions, this paper evaluate distributions of operation current, temperature rise and electromagnetic forces of gas insulated bus (GIB) plug-in connector by mechanical-electromagnetic-thermal multi-physics coupled finite element (FE) method. The FE procedure took current constriction effects among contact spots into account by imperfect contact bridge model. Effectiveness of numerical model was verified by physical experiments. Mechanical, electromagnetic and thermal behaviors of plug-in connector under various assembly conditions (preloading force, conductor insert depth and docking angle) were analyzed. Results show that due to the deviations of contact forces, operation currents and temperature rises among contact spots are not uniform. Influenced by overheating and electromagnetic force on several terrible contact spots with larger currents flow through, load capacity of plug-in connector could be reduced to 82%, 46% and 15% of design values with insufficient preloading contact force, insufficient conductor insert depth and docking angles deviation.

Index Terms ─ Electromagnetic force, finite element method, GIB, plug-in connector, short circuit current.

I. INTRODUCTION

The gas insulated bus (GIB) is favored by modern electrical industry for its large power transmission capacity, high operation reliability and well landscape coordination [1]. Spring type plug-in power connector is one of the most essential electrical connection parts inside GIB capsule. The main function of plug-in connector is to absorb misalignment caused by different thermal expansions between enclosure and conductor. However, mechanical slide able design makes the plug-in connector become weak component. As other power transmission/distribution equipment, safely operation of GIB relies on reliable connection of main electrical loop [2]. Internal insulation breakdown could be induced even contact deterioration/overheating happens on tiny part of the connector [3]. The fault of GIB equipment could be serious and power supply time is considerable due to its sealing structure. Therefore long term contact performance of plug-in connector should be accurately evaluated both in design and maintenance process to ensure safety of equipment.

Similar as other power connectors, the plug-in connector should have low and stable contact resistance and temperature rise. Mechanical structure should also be strong enough to resist the impact of short circuit current. Design-oriented closed formulas for the sliding GIB plug-in connector were given in [4], however deviation of contact performances among individual contact spots was ignored. Series works paid attention on electric, thermal and mechanical performances of power connectors during steady operation and pulse current impact by both closed formulas and numerical methods. Thermal effects of electrical contacts were analyzed by closed formulas in which the electrical connectors were modeled by lump components [5-6]. Numerical methods were conducted in order to obtain temperature distribution characteristics of electrical contacts [7-8]. Induced by current and surrounding electromagnetic field, electromagnetic repulsion forces acting on electrical connector are comprised of two parts: Holm repulsion force by the current constriction effect on contact interface [9] and Lorentz force by interaction between current carriers [10]. Focusing on electrical, thermal and mechanical field behaviors, some multi-physics models of electrical contacts were proposed in [11-12]. All of these works were based on static mechanical contact status. Forces on the contact interface were assumed as constant. However, it was noticed in [13] and our previous work [14] that transient movement on contact

Submitted On: July 31, 2017
Accepted On: April 21, 2018

interfaces of static power connector could be induced under cyclic loads such as operating current and environment temperature. Mechanical contact status of the GIB plug-in connector such as preloading contact force, conductor insert depth and docking angle can be changed with equipment service time, then make contact degeneration. Contact degeneration could reduce its load capacity. Traditional design methods paid few attentions on dynamic contact performance and load capacity of imperfect GIB plug-in connector after long time operation.

This work presents a mechanical-electromagnetic-thermal coupled physics FE method of large current GIB plug-in connector. Whole paper is organized as follows. Physical structure, test platform and numerical assumptions were described in Section 2. Multi-physics coupled FE model of imperfect assembled connector was built in Section 3. Results and experimental validation were shown in Section 4. Mechanical, electromagnetic and thermal contact behaviors of plug-in connector with various assembly conditions (preload contact force, conductor inserting depth and docking angle) under operation currents and short circuit current impact were discussed in Section 5. In Section 6, dynamic steady and fault load capacities of imperfect assembled GIB plug-in connector were discussed.

II. PHYSICAL STRUCTURE AND EXPERIMENT SET-UP

Thermal and electromagnetic force behaviors of spring type plug-in power connector used in GIB equipment were analyzed by multi-physics FE method. Physical experiments were also conducted to verify the effectiveness of the numerical model.

A. Physical structure and model assumptions

Physical structure of GIB plug-in connector is presented in Fig. 1 [4, 15-16]. GIB plug-in connector contains series pieces of contact fingers which are parallel arranged clockwise around the center axis of connector (A1). Mechanical contact forces on contact spots are supplied by series of holding springs. Conductor is made of aluminum alloy (6063-T6). The contact fingers are made of copper (T2-Y). Contact interfaces are plated with 20 μm sliver. Mechanical assembly conditions are defined as conductor insert depth H and conductor docking angle θ. Contact failure point locates on the edge chamfer of conductor plug. Geometric parameters of connector are listed in Table 1. Material properties are listed in Table 2. FE model of plug-in connector is based on the following assumptions.

- To reduce computational effort, some geometric features such as shield, bolt and other tiny chamfers (less than 0.5mm) were ignored.
- Quasi-static approximation of electromagnetic field could be used for low frequency current.
- Only mechanical contact area was considered for chemical stability of SF_6 gas. Mechanical contact was supposed occurs on one equivalent contact spot.
- During steady state analysis, electromagnetic force was omitted for its small amplitude. During short circuit fault analysis, it assumed no heat transfer occur between connector surface and environment due to the limited fault duration time.

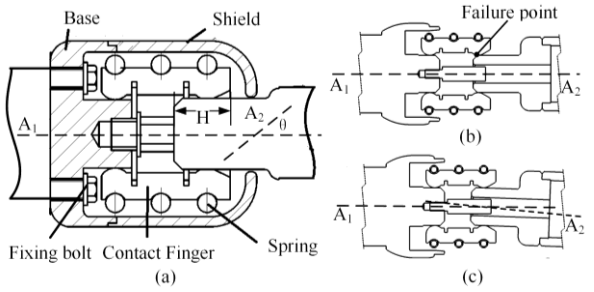

Fig. 1. Physical structure and mechanical assembly of GIB plug-in connector.

Table 1: Geometric parameters of GIB model

Conductor Material	Aluminum alloy 6063-T6
Finger Material	Copper alloy T2-Y
Conductor Length	391mm
Conductor Diameters	Φ85mm/Φ65mm
Finger Number	16
Spring Stiffness	980N/m
Spring Diameters	Φ85mm(free)/Φ108mm

Table 2: Material properties

Properties	6063	T2-Y
Density(kg/m^3)	2700	8900
Young's modulus (Gpa)	69	110
Poisson's Ratio	0.33	0.343
Resistivity (10^-8Ω.m)	3.3	1.7
Thermal conductivity(W/m/K)	209	388
Specific heat capacity (J/(kg.K))	902	391

B. Physical experiment set-up

Physical experiment set-up of prototype GIB plug-in connector was shown Fig. 2 (a). Test current was supplied by 2000A/5V current generator. Temperature rises on each contact finger were measured by k-type thermal couples. The temperature measure points were located on front sides of contact fingers nearby contact spots (Fig. 2 (b)). Analyzer was consisted of ampere meter, data acquisition (DAQ) card and Industrial Personal Computer (IPC) with LABVIEW software platform. Test currents were measured by ampere meter integrated inside the current generator. Temperatures collection interval was set as 1min.

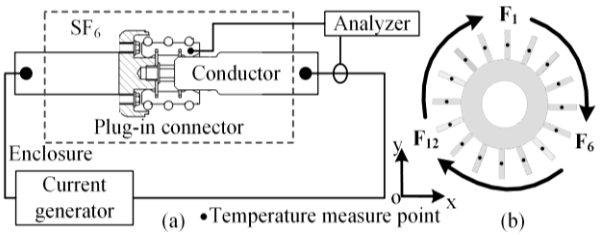

Fig. 2. Experiment set-up of GIB plug-in connector.

III. NUMERICAL MODELING

The FE analysis of GIB plug-in connector were conducted both steady state solution (operation current) and transient solution (short circuit fault). Numerical solution region is described in Fig. 3. The FE model includes contact fingers, conductors and surrounding gas medium (SF_6). Contact force F_n is influenced by the holding springs, gravity and electromagnetic force. The current I_n flows cross the contact interfaces through equivalent contact bridges.

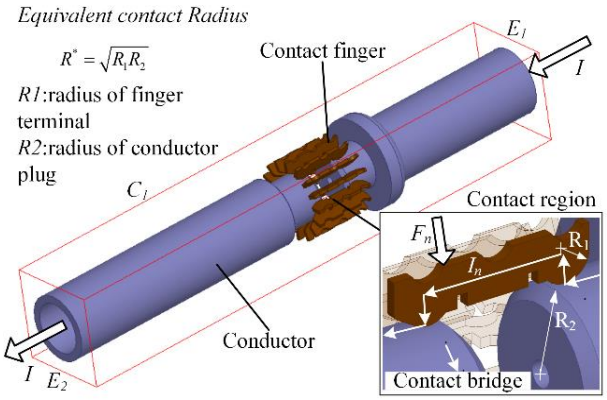

Fig. 3. Numerical solution region division and boundary conditions.

Multi-physics coupled FE analysis of GIB plug-in connector was realized by the sequent coupling (load transfer) method. Numerical calculation flowchart was described in Fig. 4. Nonlinear mechanical analysis was previous conducted to obtain initial mechanical contact parameters (forces and radiuses) on each contact spots of GIB connector with various mechanical assembly conditions. Using the radiuses $a_n(t)$ as contact bridge model parameters, electromagnetic (EM) field analysis was conducted to calculate power losses P(t) and EM force Fe(t). Temperature rise T(t) was calculated by thermal (TH) field analysis using power losses as load inputs. Contact status was updated through load step iterations during steady analysis and time iterations during transient short circuit fault analysis.

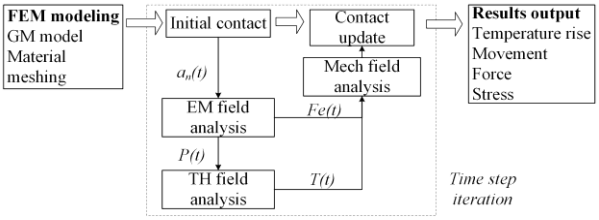

Fig. 4. Flowchart of multi-physics coupled FE procedure.

A. Field differential equations

Governing equation of electromagnetic field can be described as follows with magnetic vector potential **A**:

$$\mu\sigma\partial\mathbf{A}/\partial t - \nabla^2\mathbf{A} = \mu\mathbf{J}, \tag{1}$$

where μ is permeability, σ is electrical conductivity, $\boldsymbol{J}$ is current density. Boundary condition of electromagnetic field is as follows:

$$\mathbf{A}|_{c1} = 0. \tag{2}$$

Governing equation of thermal field can be described as follows combined with the current density as heating sources:

$$\rho c\frac{\partial T}{\partial t} - \lambda(T)\cdot\nabla^2 T = \int_V \frac{J^2}{\sigma}dV + 2\sum_{i=1}^{16} J_i^2 R_i, \tag{3}$$

where $\lambda(T)$ is thermal conductivity, ρ is material density and c is specific heat capacity, J_i is operation current on i contact spot.

Boundary conditions of thermal field include the heat fluxes on connector terminals and heat exchange between connector surface and environment:

$$\begin{cases} -\lambda(T)\dfrac{\partial T}{\partial n} = q_s \\ -\lambda(T)\dfrac{\partial T}{\partial n} = K_T(T - T_0) \end{cases}. \tag{4}$$

Equivalent heat transfer coefficient is set to consider the heat convection and radiation process:

$$K_T = (T - T_f)^{0.25} + \frac{\sigma_T \varepsilon_T}{(T - T_f)}(T^4 - T_f^4), \tag{5}$$

where σ_T is Boltzmann constant, ε_T is surface emissivity.

Self-acceleration relationship between contact resistance and contact temperature rise is as follows [17]:

$$R_c = R_0\left[1 + \frac{2}{3}\alpha_T(T - T_0)\right]. \tag{6}$$

Governing equation of mechanical field can be described as follows:

$$\begin{cases} \dfrac{\partial^2 u_i}{\partial t^2} + (\kappa + G)\dfrac{\partial e}{\partial i} = \mathbf{F_p} + \mathbf{F_g} + \mathbf{F_e} \\ \kappa = \dfrac{E\nu}{(1+\nu)(1-2\nu)} \\ e = \dfrac{\partial u_x}{\partial x} + \dfrac{\partial u_y}{\partial y} + \dfrac{\partial u_z}{\partial z} \end{cases}, \tag{7}$$

where u_i is the direction deformation along components of Cartesian coordinate system (i=x, y, z), κ is the lame constant, G is shear modulus, e is volume deformation, external forces include preloading force $\mathbf{F_p}$, conductor gravity $\mathbf{F_g}$ and electromagnetic force $\mathbf{F_e}$.

Pre-loading contact force on per contact spot can be expressed as:

$$F_p = 3K\pi^2 \Delta D / n, \tag{8}$$

where K is the spring stiffness and ΔD is the spring diameter increase after assembly.

Electromagnetic force induced by the interaction between current and magnetic field can be expressed as:

$$F_e = \int_V J \times B dV. \tag{9}$$

The GIB plug-in connectors are often fixed on the disc-type insulators, and the positioning design allows only axial freedom (direction of insert depth) and limited range of radial freedom (less than 2°).

Backward stepping scheme is adopted for the time discretization during the transient short circuit analysis:

$$(dx / dt)^{t+\Delta t} = (x^{t+\Delta t} - x^t) / \Delta t, \tag{10}$$

where x is the field nodal variables, t is the analysis time, the time step Δt is set as 1ms to simulate transient short circuit fault process.

B. Contact equivalent

The mechanical contact radius a_n on individual contact spot can be calculated by Hertz formula:

$$a_n = (3F_n R^* / 4E^*)^{1/3}, \tag{11}$$

where F_n is the contact force of n contact finger which equals to half of reactive force on individual contact spots, R^* is the equivalent contact radius (Fig. 3), E^* is equivalent Young's modulus.

The role of current constriction effect and contact resistance is usually considered by the contact bridge model. However, forces and radii on several contact spots are too small to be geometrically modeled. To simply contact spots of GIB plug-in connector under various assembly conditions, imperfect contact bridge model was constructed in our previous work [18] by two parameters: the equivalent contact radius r_n and the equivalent electric resistivity ρ_n:

$$\begin{cases} r_n = a_n & a_n \geq 0.1mm \\ r_n = 0.1mm & a_n < 0.1mm \end{cases}, \tag{12}$$

$$\rho_n = \eta \rho_{\text{silver}}, \tag{13}$$

$$\begin{cases} \eta = 1 & a_n \geq 0.1mm \\ \eta = 0.1 / a_n & 0 < a_n < 0.1mm \\ \eta = \infty & a_n = 0mm \end{cases}, \tag{14}$$

where η is electric resistivity ratio between n contact bridge and silver.

IV. FIELD RESULTS AND VERIFICATION

3-D FE model of GIB plug-in connector was built to describe mechanical, electrical and thermal field behaviors of GIB plug-in connector under operation current and short circuit current impact. The mechanical assembly condition was defined as 30mm of conductor insert depth, 0° of conductor docking angle under initial preloading contact force. Environmental temperature was 18℃. Operation current was 2000A and typical transient waveform of short circuit current was as follows:

$$i(t) = \sqrt{2} I (e^{-\alpha t} - \cos(\omega t)), \tag{15}$$

where I=10kA, ω=100π, α=22.311s^{-1}.

A. Field distributions

Mechanical field distribution of GIB plug-in connector is described in Fig. 5. Results show that the radial deformation happens on contact fingers for the over-travel design between connector and conductor terminal. Deformations on bottom contact finger are larger than upper ones for gravity. Influenced by uneven deformation of contact elements, mechanical stresses concentrate on contact spots and the maximum stress increasing from upper contact spots to bottom ones. Uneven mechanical contact forces can influence distributions of contact resistances and currents.

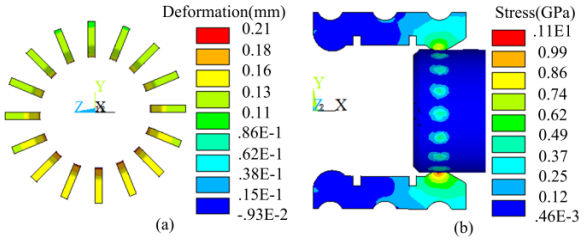

Fig. 5. Initial mechanical field distributions: (a) radial deformation and (b) von-Mises stress.

Distributions of current densities and temperature rises of GIB plug-in connector are described in Fig. 6. Results show that current density concentrates on contact spots for the limited electrical contact area. Local power losses and excessive temperature rises on contact spots can be induced by current. Temperatures on the bottom contact fingers are larger than those of upper ones for the deviation of operation current which is influenced by mechanical contact forces. It can be deduced that the mechanical assembly conditions could influence the thermal behaviors and load capacities of GIB plug-in connector.

Current and electromagnetic force densities of GIB plug-in connector concerning under peak value of short circuit current (t=10ms) are shown in Fig. 7. Results show the currents of lower contact fingers are larger than those of upper ones, which causes non-uniform electromagnetic forces. The electromagnetic force on contact finger is opposite to the preloading contact force. Real contact force can be reduced by increasing of

electromagnetic force under short circuit fault.

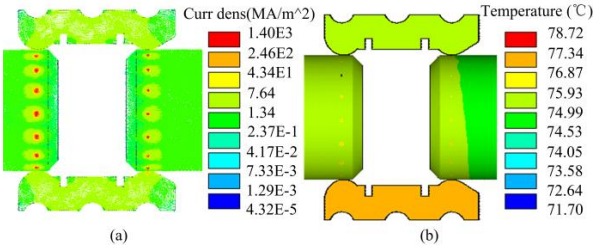

Fig. 6. Steady current and temperature distributions.

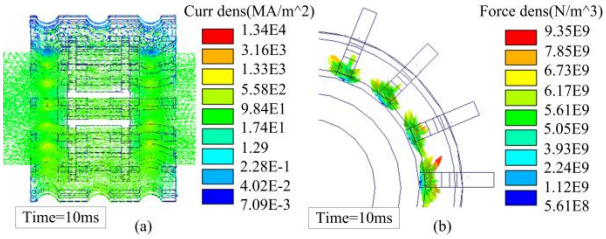

Fig. 7. Current and electromagnetic force distributions.

B. Transient characteristics under short circuit fault

Transient thermal responses of contact spot and conductor terminal under short circuit current impact are described in Fig. 8. Results show that temperature on contact spot follows the waveform of short circuit fault current for the small thermal constants. However, unlike contact spot, the transient temperature rise on measure points does not follow the fault current for the relative large thermal constants. Similar result has been found by research on similar connector structure [19].

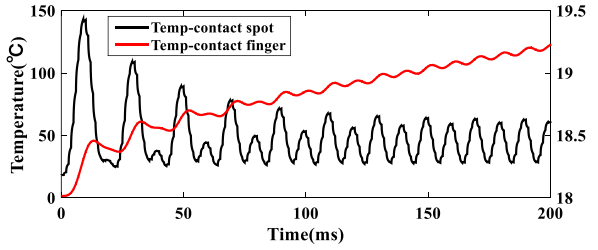

Fig. 8. Thermal response at contact spot and conductor.

Figure 9 shows the transient electromagnetic forces and temperature on the bottom contact spot (no.9 in Fig. 2) within the first three waveforms of fault current (60ms). FE results are compared with the well-known V-T relation [20] and design formula [4]. Results show that temperature by FE analysis lags behind the V-T relation for the difference between electric and thermal time constants of contact spot. Electromagnetic force contains 50Hz and 100Hz components, and force amplitudes by design formula are 50% smaller than FEM results for the Lorentz force is not considered.

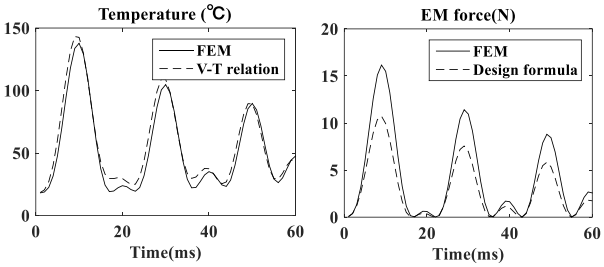

Fig. 9. Transient temperature rises and electromagnetic force on the bottom contact spot.

C. Results verification

Physical experiments were carried out in order to verify effectiveness of numerical model besides provide more information about thermal performance of GIB plug-in connector. Steady-state temperature rises on individual contact spots under different operation currents were obtained by both FE model and physical experiments. Calculated and the measured results are listed in Table 3. Both calculated and measured results follow the same trend as described in Fig. 6. The maximum deviation of calculation and test results is less than 15%. Errors are caused by approximation of heat transfer coefficient. Several thermal couples could be loosen due to higher test temperature.

Table 3: Temperature on individual contact spots (℃)

No	1000A		2000A		3000A	
	FEM	Test	FEM	Test	FEM	Test
1	35.4	36.3	58.6	66.9	92.4	105.2
2	36.2	36.3	60.6	67.1	100.0	105.3
3	36.4	36.4	63.3	68.4	100.1	106.1
4	36.6	36.6	65.3	68.8	101.6	106.9
5	37.4	36.8	65.8	70.6	103.4	108.0
6	37.5	36.9	66.7	71.8	104.5	108.9
7	38	37.1	67.4	72.6	105.0	109.6
8	38.8	37.1	71.7	73.0	105.2	110.0
9	38.3	37.2	73.8	73.2	107.8	110.2
10	38.1	37.1	68.8	73.1	107.1	110.1
11	37.7	37.0	67.2	72.4	106.2	109.4
12	36.4	36.9	66.8	71.8	104.6	109.0
13	36.3	36.8	65.9	70.7	101.3	108.2
14	35.8	36.6	63.4	68.8	99.6	107.1
15	35.5	36.4	62.9	67.4	97.5	106.1
16	35	36.3	60.9	66.7	92.6	105.5

V. CONTACT BEHAVIORS WITH VARIOUS ASSEMBLY CONDITONS

Distributions of mechanical contact parameters among contact spots across total assembly ranges are critical for electrical and thermal performance of GIB

plug-in connector. Using mechanical field analysis, distributions of initial mechanical contact forces and radii of plug-in connector with different mechanical assembly conditions are described in Fig. 10. Results show mechanical contact parameters on individual contact spots vary from each other. Deviation of contact parameters becomes larger with decrease of preloading contact forces, conductor insert depths, and increasing of conductor docking angles. Influenced by mechanical contact parameter deviations, contact resistances and currents among contact spots are different.

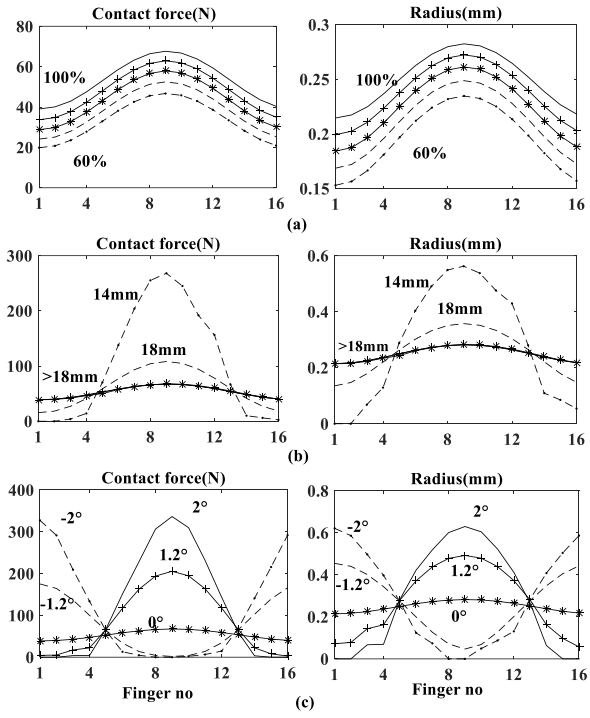

Fig. 10. Distributions of contact forces and radii: (a) preloading contact force, (b) conductor insert depths, and (c) conductor docking angle.

A. Contact behaviors under steady-state

Operation current up to several kA can lead to obvious temperature rise on contact spots. Ampacities of plug-in connector are constrained by the maximum temperature. Distributions of currents and temperature rises of GIB plug-in connector with different assembly conditions under 2000A current at 18℃ environmental temperature are shown in Fig. 11.

Distribution of currents and temperatures among contact spots with various preloading contact forces are described in Fig. 11 (a). Results show that the reducing of preloading contact forces by lower spring stiffness could make larger current deviations, which induce larger temperature rise on the bottom contact spots. However, the maximum temperature (94.5℃) could not exceed threshold (105℃), even the preloading contact force decrease to 60% of its initial value; which means that reducing of preloading contact force is not the main factor influencing contact performance of connector under steady-state operation current.

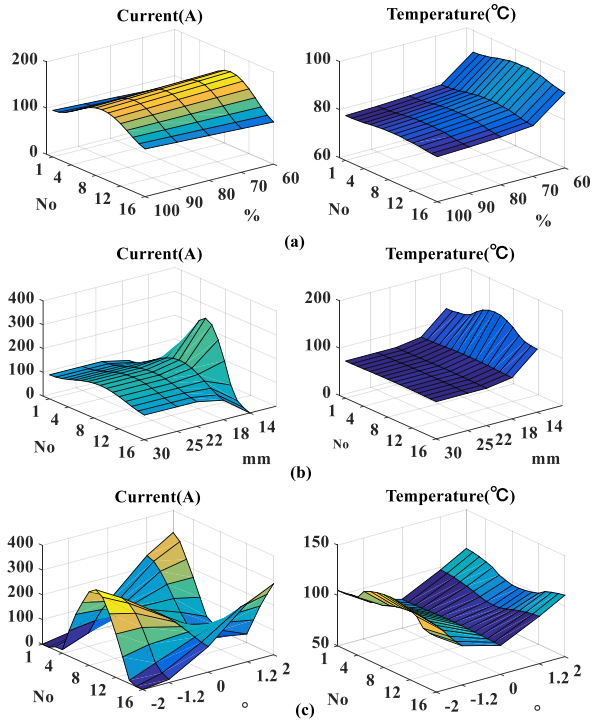

Fig. 11. Currents and temperatures on individual contact spots of GIB plug-in connector under steady state.

Distribution of currents and temperatures among contact spots with various conductor insert depths are described in Fig. 11 (b). Results show that deviation of currents and temperatures become larger with decrease of conductor insert depths. When conductor insert depth does not exceed failure point (18mm), the maximum temperature is below threshold value for nearly uniform contact parameters. However, when conductor insert depth exceeds failure point, current and temperature among contact spots significantly deviates. Overheating could be induced on several spots with larger currents.

Distributions of currents and temperatures among contact spots with various conductor docking angles are described in Fig. 11 (c). Results show that deviation of temperature becomes larger with increase of conductor docking angles. When docking angle deviation is below 1.2°, the maximum temperature is below threshold value for nearly uniform contact parameters. However, when conductor docking angle deviation exceeds 1.2°, temperature among contact spots significantly deviates. Overheating could be induced on several contact spots with larger currents flowing through. The maximum temperature at -2° docking angle is 11.3℃ larger than that at 2° docking angle due to the conductor gravity.

B. Contact behaviors under short circuit fault

Peak value of fault current under short circuit can reach up to tens of kA. Huge electromagnetic repulsion force and sharp increasing of temperature rise could be induced. Distributions of electromagnetic force and temperature of GIB plug-in connector with different assembly conditions under 25kA fault current impact at 18℃ environmental temperature are shown in Fig. 12.

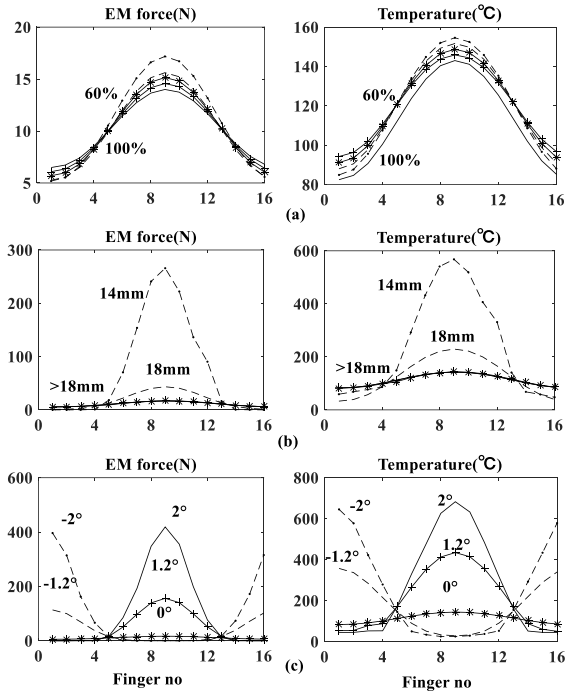

Fig. 12. Electromagnetic force and temperature under short circuit current impact.

Distributions of electromagnetic repulsion forces and temperatures among contact spots with various preloading contact forces are shown in Fig. 12 (a). It can be seen that deviation amplitudes of electromagnetic force and temperature increase with the decrease of preloading contact forces. However, even when the preloading contact force reduces to 60% of its initial value, the residual contact force still exists with the peak value of electromagnetic repulsion force (17.2N). The maximum temperature (154.6℃) does not exceed the threshold (200℃), which means that reducing of preloading contact force is not the main factor influencing contact performance under short circuit current impact.

Distributions of electromagnetic repulsion forces and temperatures among contact spots with various conductor insert depths are shown in Fig. 12 (b). It can be seen that deviation amplitudes of electromagnetic force and temperature rise increase with decrease of conductor insert depth. Preloading contact force on several serious contact spots could be totally offset by electromagnetic force together with seriously heating at 14mm conductor inserting depth, which means that the contact performance could be largely reduced by the insufficient conductor insert depth.

Distributions of electromagnetic repulsion forces and temperatures among contact spots with various conductor docking angles are shown in Fig. 12 (c). Results show that deviation of electromagnetic and temperature becomes larger with increase of conductor docking angles. When docking angle deviation exceeds 1.2°, preloading contact force on several serious contact spots could be totally offset by electromagnetic force, which means that the contact performance could be largely reduced by conductor docking angle deviation.

VI. LOAD CAPABILITY ASSESSMENT OF IMPERFECT PLUG-IN CONNECTOR

As part of series components in power grid, during entire equipment service life, contact system of GIB plug-in connector must be able to carry rated operation current besides withstand short circuit (SC) fault current without obvious contact degradation. According IEC 62271-1 and IEC 60865-1 [21-22], the maximum allowed temperatures for silver-plated contacts with long-term operation current and transient short circuit current impact is 105℃ and 200℃ separately.

During manufactory/install/operation process, GIB plug-in connector could be exposed to misalignment conditions such as preloading contact force reduction, insufficient conductor insert depth or conductor docking angle deviation. Imperfect assembly conditions could make higher temperature rise and electromagnetic force thus reduce the actual load capability comparing with its design value.

Load capabilities of GIB plug-in connector with various preloading contact forces are described in Fig. 13. Results show that the load capabilities reduce with decrease of preloading contact force. Load capacity of connector with 60% preloading contact force is 82% of its design value, which means that preloading contact force could not obviously influence load capability of connector with low relaxation ratio of holding spring across its service life.

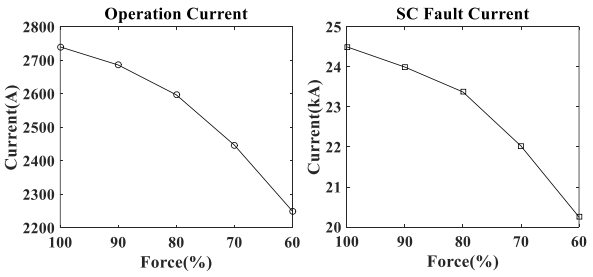

Fig. 13. Load capacities with preloading contact forces.

Load capabilities of GIB plug-in connector with various conductor insert depths are described in Fig. 14. Results show that as long as the conductor insert depth is below contact failure point (18mm), load capacities reduce slowly with decrease of conductor insert depth (87% of its design value at 18mm). However, when the conductor insert depth exceeds failure point, due to overheating and significant electromagnetic force on several contact spots, the load capacities reduce sharply (46% of initial value at 14mm).

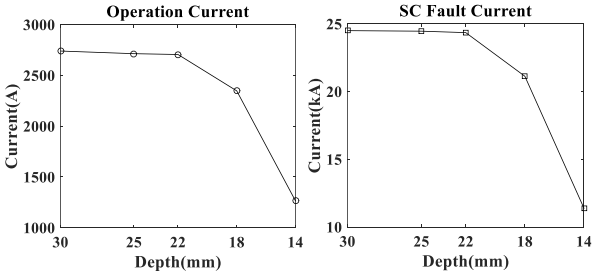

Fig. 14. Load capacities with conductor insert depths.

Load capabilities of GIB plug-in connector with various conductor docking angles are described in Fig. 15. Results show that due to overheating and significant electromagnetic force on several contact spots, the load capacities reduce sharply with the increase of conductor docking angle (15% of its design value at -2°).

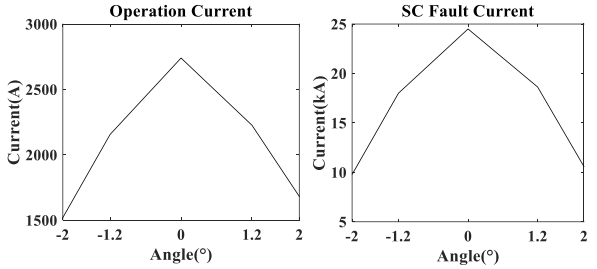

Fig. 15. Load capacities with conductor docking angles.

VII. CONCLUSION

By multi-physics coupled FE procedure, influences of imperfect assembly conditions on the mechanical, electrical and thermal contact behaviors of GIB plug-in connector under steady and short circuit current impact have been analyzed. Results show that when imperfect assembly condition happens, contact force, operation current, temperature rise and electromagnetic repulsion force deviate obviously among contact spots. The load capacity can be significant decreased by overheating on several contact spots. When insufficient preloading force (60%), insufficient conductor insert depth (14mm) and conductor deviation angle (-2°) happen, the actual load capability reduces to 82%, 46% and 15% of its design values. Result also indicates that insufficient conductor inserts depth and conductor docking angle deviation has the larger influence on load capacity of connector. FE model and results of this paper could help for optimal design and operation monitoring of GIB plug-in connector thus improve its reliability.

ACKNOWLEDGMENT

This work was supported by the Natural Science Foundation of China (51607124), the 60th China Postdoctoral Science Foundation (2016M602352), and the Fundamental Research Funds for China Central Universities (2042016kf1049, 2042017kf1011).

REFERENCES

[1] K. Mark, W. Christian, and G. Alfred, "The latest GIS and GIL developments for high voltage applications," *Proc. ICHVE*, pp. 56-59, 2008.

[2] M. Runde, "Failure frequencies for high-voltage circuit breakers, disconnectors, earthing switches, instrument transformers, and gas-insulated switchgear," *IEEE Trans. Power Delivery*, vol. 28, no. 1, pp. 529-530, 2013.

[3] Y. Mukaiyama, I. Takagi, K. Izumi, T. Sekiguchi, et al., "Investigation on abnormal phenomena of contacts using disconnecting switch and detachable bus in 300 kV GIS," *IEEE Trans. Power Delivery*, vol. 5, no. 1, pp. 189-195, 1990.

[4] A. E. Emanuel, H. C. Doepken, and P. C. Bolin, "Design and test of a sliding plug-in conductor connector for compressed gas-insulated cables," *IEEE Trans. Power Apparatus and Systems*, vol. 95, no. 2, pp. 570-579, 1976.

[5] M. P. Filippakou, C. G. Karagiannopoulos, D. P. Agoris, and P. D. Bourkas, "Electrical contact overheating under short-circuit currents," *Electric Power Systems Research*, vol. 57, no. 2, pp. 141-147, 2001.

[6] L. Koller, B. Novák, and G. Tevan, "Heating effects of short-circuit current impulses on contacts and conductors," *IEEE Trans. Power Delivery*, vol. 23, no. 1, pp. 221-227, 2008.

[7] B.-K. Kim, K.-T. Hsieh, and F.-X. Bostick, "A three-dimensional finite element model for thermal effect of imperfect electric contacts," *IEEE Trans. Magnetics*, vol. 35, no. 1, pp. 170-174, 2009.

[8] O. Bottaushort, "Numerical analysis of heating transient of electric contacts under short-circuit conditions," *IEEE Trans. Comp. Hybrids Manufact. Technol.*, vol. 16, no. 5, pp. 563-570, 1993.

[9] T. Ota, S. Suzuki, and K. Hirata, "Dynamic analysis method of repulsion forces on current-carrying contact using 3-D FEM," *IEEE Trans. Magnetics*., vol. 47, no. 5, pp. 942-945, 2011.

[10] S. Ito, Y. Takato, Y. Kawase, and T. Ota, "Numerical analysis of electromagnetic forces in low voltage ac circuit breakers using 3-D finite

element method taking into account eddy currents," *IEEE Trans. Magnetics*., vol. 34, no. 5, pp. 2597-2600, 1998.
[11] E. Carvou, R. EI Abdi, J. Razafiarivelo, N. Benjemaa, and E. M. Zindine, "Thermo-mechanical study of a power connector," *Measurement*., vol. 45, no. 5, pp. 889-896, 2012.
[12] A. Monnier, B. Froidurot, C. Jarrige, et al., "A mechanical, electrical, thermal coupled-field simulation of a sphere-plane electrical contact," *IEEE Trans. Comp. Packing Technol*., vol. 30, no. 4, pp. 787-795, 2007.
[13] Y.-Z. (Liza) Lam, J. W. McBride, C. Maul, and J. K. Atkinson, "Displacement measurements at a connector contact interface employing a novel thick film sensor," *IEEE Trans. Comp. Packing Technol*., vol. 31, no. 3, pp. 566-573, 2008.
[14] G. Xiangyu, S. Naiqiu, K. Bing, et al., "Multi-physics calculation and contact degradation mechanism evolution of GIB connector under daily cyclic loading," *IEEE Trans. Magnetics*., vol. 52, no. 3, pp. 1-4, 2016.
[15] Y. Ohshita, A. Hashimoto, and Y. Kurosawa, "A diagnostic technique to detect abnormal conditions of contacts measuring vibrations in metal tank of gas insulated switchgear," *IEEE Trans. Power Delivery*, vol. 4, no. 4, pp. 2090-2094, 1989.
[16] L. Bin, *SF6 High Voltage Electrical Design.* BeiJing, China Machine Press, 2007.
[17] J. Paulke, H. Weichert, and P. Steinhaeuser, "Thermal simulation of switchgear," *IEEE Trans. Comp. Packing Technol.*, vol. 25, no. 3, pp. 434-439, 2002.
[18] G. Xiangyu, S. Quanyu, et al., "Investigation on mechanical and magnetic field behaviors of GIB plug-in connector under different contact conditions," *Appl. Comp. Elec. Society Journal*, vol. 32, no. 3, pp. 275-282, 2017.
[19] M. Gatzsche, N. Lucke, S. Grobmann, T. Kufner, and G. Freudiger, "Evaluation of electric-thermal performance of high-power contact systems with the voltage-temperature relation," *IEEE Trans. Comp. Packing Manu. Technol*., vol. 7, no. 3, pp. 434-439, 2017.
[20] R. Holm, *Electric Contacts, Theory and Applications.* New York, Springer, 1979.
[21] High-Voltage Switchgear and Control Gear—Part 1: Common Specifications, Document IEC 62271-1 Edition 1.1 2011-08, 2011.
[22] Short-Circuit Currents—Calculation of Effects—Part 1: Definitions and Calculation Methods, Document IEC 60865-1 Edition 3.0 2011-10, 2011.

Xiangyu Guan received the B.S. degree of Environmental Science from Xinjiang Normal University, China, in 2010, the M.S. and Ph.D. degrees of Power System and Automation from Wuhan University, Hubei, China, in 2015.

He is currently a Lecturer at School of Electrical Engineering Wuhan University. He is Member of ACES and ICS and his research interests mainly focus on electrical contacts, numerical methods of coupling field calculation and condition monitoring of electrical equipment.

Xin Wei received her B.S. degree of Electrical Engineering from Fuzhou University, China, in 2016. She is currently a master candidate in School of Electric Engineering in Wuhan University. Her research interests include online monitoring technology and fault diagnosis of electric equipment.

Xianyong Song received the B.S. degree of Electrical Engineering from Hunan University, China, in 1994, the M.S degree in School of Electrical Engineering Wuhan University, Hubei, China, in 2015. He is currently a Senior Engineer in State Grid Hunan Power Supply Company and his research is working on electrical equipment monitoring and fault diagnosis technology.

Naiqiu Shu received the M.S. and Ph.D. degrees in Electrical Engineering from Wuhan University. He is currently a Professor in School of Electrical Engineering Wuhan University. His current research interests mainly focus on sensors technology and its application on condition monitoring of electrical equipment.

Hui Peng received the B.S., M.S. and Ph.D. degrees in Electrical Engineering from Wuhan University. He currently is an Associate Professor in School of Electrical Engineering. His current research interests mainly focus on condition monitoring of electrical equipment.